Available online at www.sciencedirect.com
SCIENCE DIRECT®
Journal of Sound and Vibration 282 (2005) 61–87
JOURNAL OF SOUND AND VIBRATION
www.elsevier.com/locate/jsvi

A statistical model for landing gear noise prediction

Yueping Guo*

The Boeing Company, Mail Code H013-B308, 5301 Bolsa Avenue, Huntington Beach, CA 92647, USA

Received 8 August 2003; accepted 14 February 2004
Available online 22 September 2004

Abstract

This paper presents the development of a framework for aircraft landing gear noise prediction. A prediction model is derived that decomposes the landing gear noise into three spectral components, for the low, mid and high frequencies, respectively. This corresponds to cataloguing the parts in the landing gear assembly into three groups, namely, the wheels for low frequencies, the main struts for mid frequencies and the small details for high frequencies. The spectral decomposition is demonstrated by experimental data from a full-scale Boeing 737 landing gear test, which show different spectral characteristics of the noise in the three different frequency domains. In each frequency domain, asymptotic results are derived for the farfield noise, by making use of different length scales to simplify the phase behavior of the sources. The derived results require as input only some statistical descriptions of the surface pressure fluctuations and the geometry of the landing gear assembly. Some simple examples are given to demonstrate the features of the predicted noise, which show trends consistent with experimental data. The frequency domain decomposition also points to simple ways of obtaining the surface pressure properties required for noise prediction, which is also discussed in this paper.
© 2004 Elsevier Ltd. All rights reserved.

1. Introduction

Landing gear noise has been attracting a lot of attention in recent years because it is now recognized as one of the major components of airframe noise for commercial aircraft. It is also

*Tel.: 714-8961527; fax: +1-714-8961559.
E-mail address: yueping.guo@boeing.com (Y. Guo).

0022-460X/$ - see front matter © 2004 Elsevier Ltd. All rights reserved.
doi:10.1016/j.jsv.2004.02.021

Nomenclature

a	typical dimension of cross-section
$\mathbf{A}$	transformation matrix from global to local coordinates
B	longitudinal correlation function of surface pressures
c	constant sound speed
C_j	cross-section contour of jth component
d	main strut diameter
D	wheel diameter
F_i	total force on landing gear in ith direction
$F_i^{(j)}$	sectional force on jth component in ith direction
k	acoustic wavenumber
L_j	length of jth component
M	flow Mach number
$\mathbf{n}_f$	unit vector of sectional force
n_i	surface normal in ith direction
N	total number of components
p	acoustic pressure
p_c	circumferentially averaged surface pressure
p_s	surface pressure on gear component
q	dynamic head
s	arc length coordinate
s_0	arc length coordinate at stationary point
S	total surface area
S_j	surface area of jth component
St	Strouhal number
St_d	Doppler-shifted Strouhal number
$\mathbf{t}$	surface tangent vector
t	time
U	mean flow velocity
U_c	convection velocity normal to length direction
V_c	convection velocity in length direction
x_i	coordinates fixed on ground
y_i	source coordinates
z_i	local coordinates
Δ	Doppler factor
$\Phi^{(j)}$	auto-coherence of sectional forces
Π	noise spectrum
η	moving coordinates
ρ	constant mean density
τ	source time
ω	angular frequency
ψ	phase function

one of the most difficult noise components to understand, predict and suppress. This is because the mechanisms responsible for the noise radiation involve complex flows in a complex geometry setting, which makes detailed studies, experimental and/or numerical, very difficult. Consequently, it can be expected that in the foreseeable future, practical noise prediction for landing gears will either heavily rely on empiricism or involve acceptable approximations to simplify the problem. In this paper, we follow the latter approach to develop a statistical framework for landing gear noise prediction. In essence, our methodology decomposes the landing gear noise spectrum into three frequency domains, which are denoted as the low-, the mid- and the high-frequency domain, respectively. The components in the landing gear assembly are grouped according to their main noise contributions in these three frequency domains. Noise prediction for each frequency component is derived asymptotically by making use of statistical descriptions of the flow properties, such as their ensemble-averaged cross and auto spectra, to avoid detailed deterministic computation of the nearfield flow. The entire frequency domain of practical interest can be covered by empirically matching these asymptotic results and the total noise is predicted by statistical energy addition of the noise contributions from individual parts of the landing gear assembly.

The frequency domain decomposition enables us to derive analytical solutions because the noise sources behave quite differently in these different frequency domains. The aggregate effects of the distributed sources on the farfield radiation critically depend on the relative phases of the sources. For low frequencies, the typical sound wavelength is longer than the dimensions of the landing gear components so that the phase variation of the sources is small across the landing gear assembly. In this case, the far field sees all sources in phase and the source distribution is equivalent to a concentrated source. This is in fact the extensively studied case of sound from compact bodies where the compactness is measured by the acoustic wavelength [1–4]. In this case, noise prediction only requires information on the total forces on the landing gear assembly. In the much less studied case of high frequencies, the phases of the sources vary significantly across the source distribution. This rapid phase variation leads to some mutual cancellation of the radiated sound. As a result, the farfield noise is dominantly generated by sources at locations where their phase variation vanishes. In this case, noise prediction only requires information at a few locations in the source distribution. Whether the sources are compact or non-compact depends on the ratio of a physical dimension to the acoustic wavelength. For a typical elongated landing gear component such as a strut, its length may be longer than the acoustic wavelength but its cross-section dimension may be compact. This is what we call the low-frequency domain, in which different approximations apply in the two different length scales. These different kinds of source behavior in different frequency domains are represented by a phase function of the sources in the frequency domain version of the Ffowcs Williams/Hawkings equation [5], which has been applied to various aeroacoustics problems [6–8]. We will show that in each frequency domain, different approximations can be applied to this phase function, which enables the derivation of analytical solutions for the farfield sound.

We choose to work with frequency domain decomposition, not only because this approach enables us to derive simple analytic results for each spectral component, but also because these spectral components correspond to noise generated by different groups of landing gear parts. To demonstrate this, we will discuss some experimental data, obtained in an acoustic test for a full-scale Boeing 737 landing gear [9]. The experiment was done in such a way that contributions from the wheels, the main struts and the detailed dressings such as hoses and wires can be easily separated from each other. It will be shown that the three groups of landing gear components generate noise with quite different spectral characteristics, mostly controlled by their respective length scales.

While noise from the wheels and main struts have been studied in the past [4,10,11], the smaller components such as the hoses and wires associated with the hydraulic system and the small cutouts and steps have not received as much attention. It is only in recent years that these small parts were recognized as very important contributors to the high-frequency noise [12,13], which is the most important component in aircraft noise certification. Because of this, existing prediction tools, mostly based on studies on wheel and strut noise, usually underpredict the total landing gear noise, especially for practical noise metrics such as the effective perceived noise level (EPNL), a standard measure for aircraft noise. This is because high-frequency noise is heavily weighted in calculating this noise metric, but is missing in predictions based on wheel and strut noise. To demonstrate this, we will use the Boeing 737 landing gear as an example and show that prediction tools currently in use [11] underpredict landing gear noise by as much as 7 EPNL dB. We will also show that this large amount of underprediction is mostly from the high-frequency domain. This

clearly points to the need for prediction tools with high-frequency capability. Unfortunately, high-frequency noise is also a very difficult component to work with because of the small length scales associated with the high-frequency sources. This is why we choose to work with an approximate approach based on asymptotic analysis.

The results of this approach, while admittedly not precise in details can be useful in many aspects. The first is its prediction capability for practical applications. We will derive formulas that only require statistical descriptions of the flow field, such as the cross and auto coherence of the surface pressures, and the geometry of the landing gear assembly. The computational requirement for computing the noise is quite trivial. The second useful aspect of this approach is the revelation of functional dependencies of landing gear noise on flow and geometry parameters. These functional dependencies are controlled by the physical mechanisms that are responsible for the noise generation, and hence, point to directions for potential technology development for noise reduction. Because our approach involves making a series of approximations to the exact, complete problem, the procedure provides a hierarchy of prediction tools with various degrees of accuracy. The intermediate results in the derivation can all be regarded as prediction tools whose usefulness depends on the degree of accuracy required and the completeness of the available flow information. The theoretically most accurate case is where all the flow information is known exactly. In such a theoretical case, the complete Ffowcs Williams/Hawkings equation [5] provides precise predictions for the noise. Apparently, such precise predictions are not available at the present time for practical applications. At the other end of this hierarchy, the formulas that require the least input information are those using empirical data for the flow statistics. It is conceivable that in the future this kind of flow statistics can be derived from more detailed simulation, instead of pure empirical curve fitting.

The approach followed here to derive the noise prediction formulas is precisely in the spirit of the Lighthill acoustic analogy [14], namely, by assuming that the nearfield flow information is obtainable independent of the acoustic field. This can be justified by the low flow Mach number typical of landing gear noise applications, where the flow-generated noise simply propagates away from the gear without much backreaction on the flow. The asymptotic analysis in the three frequency domains not only leads to explicit analytical formulas for noise prediction, which is very desirable for engineering applications, but also points to simple ways to obtain the nearfield information required for noise prediction. This is because the noise from different frequency domains is generated by different groups of landing gear parts. This, together with some assumptions concerning the mutual interactions between the parts, makes it quite feasible to obtain the required nearfield flow properties without full-blown numerical simulations for realistic landing gears or large-scale detailed high-fidelity landing gear tests. This will be discussed in this paper.

2. Some experimental observations

To demonstrate how the components in the landing gear assembly generate noise in different frequency domains and to show the characteristics of the generated noise in these respective frequency domains, we discuss some experimental data in this section. The data were obtained from an acoustic test in the Boeing Low Speed Aeroacoustics Facility (LSAF). The test was done

for a full-scale model of a Boeing 737 landing gear with farfield noise measurements made by both free field microphones and by a phased microphone array. The free field microphone measurements, which are the data discussed in this paper, cover the emission angle range from 65° to 150°, the directivity angle being measured from the upstream direction. Details of this test have been previously reported [9] so that only relevant data are discussed here.

The landing gear was tested in various configurations and flow conditions. Flow conditions vary with Mach number ranging from 0.18 to 0.24. For the gear configurations, three are of particular interest to us, namely, the dirty, the clean and the no-wheel configuration. The dirty configuration is a fully dressed landing gear with all the small parts such as the hoses and wires from the hydraulic system. Thus, its noise is the total noise for this landing gear. The clean configuration is a simplified gear consisting of only the wheels and the main struts. This is typical of the configurations studied in small-scale experiments in the past. The no-wheel configuration consists of only the struts. These three configurations are interesting because the difference between any two of them yields noise from a particular group of components in the landing gear assembly. We will take the clean configuration as our baseline, which mainly radiates low- and mid-frequency noise because the wheels and main struts have relatively large length scales. When taking the difference between the dirty and the clean configuration, the results are the noise from the small components such as hoses and wires, which is mainly in the high-frequency domain. Similarly, low-frequency noise from the wheels can be found by taking the difference between the clean and the no-wheel configuration.

This source separation is illustrated in Fig. 1, which shows a typical noise spectrum for the Boeing 737 landing gear, plotted as sound pressure level in one-third-octave bands. The top curve (without any symbols) is the total noise and the different components in different frequency

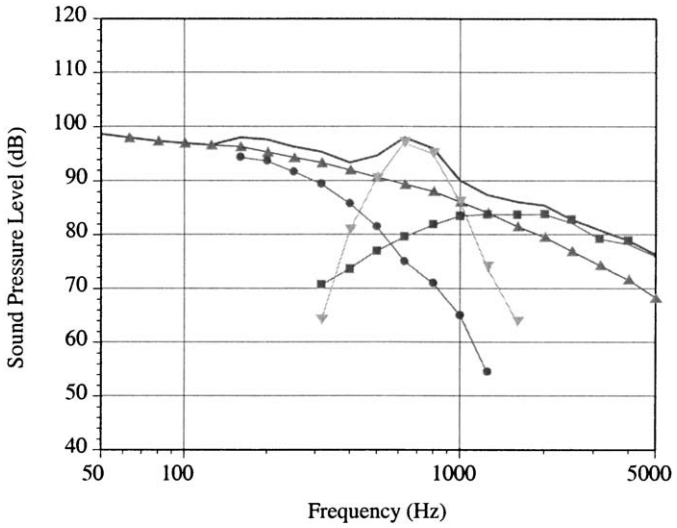

Fig. 1. Illustration of a typical noise spectrum of the Boeing 737 landing gear and its decomposition into different components: ●●●, from wheels; ▲▲▲, from main struts; ■ ■ ■, from small details; ▼▼▼, from an unknown source and the solid curve represents the total noise.

domains are plotted and identified by the symbols. The curve for the baseline, clean configuration noise (low and mid frequency), is identified by the up-pointing triangles. This is used as the baseline to derive other components, the high-frequency component (squares) from the difference between the dirty and clean configuration and the very low-frequency component (circles) from the difference between the clean and the no-wheel configuration. The low-frequency noise component is seen to be dominant around and below about 100 Hz and decreases very rapidly with increasing frequency. It can be seen from Fig. 1 that the mid-frequency component also decreases with frequency, but at a much more gradual rate. Thus, in the frequency range between about 100 and 600 Hz, it is the dominant noise source. In the frequency band between about 600 and 1000 Hz, there is a spectral hump shown in Fig. 1, which we have marked by the down-pointing triangles. This hump, however, does not appear in any consistent way in the test. Furthermore, by studying the functional dependencies of the noise on flow conditions and configurations, we have not noticed any consistent trend associated with this hump. Thus, we have not been able to conclude whether it is from any real landing gear noise source. For the discussions in this paper, we will ignore this hump. As a result, the mid-frequency component can be regarded as dominant in the frequency range between 100 and 1000 Hz.

It is clear from Fig. 1 that the dominant noise for frequencies above 1000 Hz is mainly from the small parts in the landing gear assembly. For these frequencies, the dirty configuration is much noisier than the clean configuration. This leads to two important conclusions. One is that prediction tools for landing gear noise must have high-frequency capability because it is the most important frequency domain for aircraft noise certification. Unfortunately, almost all the prediction tools currently in use do not have this capability. In the past, most empirical predictions have been based on model gear tests that only involved landing gear wheels and the main struts connecting them [4,10,11]. This is basically the clean configuration we are considering and only gives the low- and mid-frequency noise. Clearly, the small parts such as the hoses, wires, cutouts and steps are difficult to implement in small-scale models. Thus, accurate empirical predictions of landing gear noise for practical applications should rely on full-scale tests or high-fidelity large-scale model tests, such as those done in recent years [12,13]. For numerical and analytical prediction, the high-frequency domain clearly poses an extremely difficult task, because of the complexity of the small parts in the gear, their small length scales and the small time scales of the sound waves they generate. Though much progress has been made in recent years in Computational Fluid Dynamics (CFD) and Computational Aeroacoustics (CAA), numerical prediction of landing gear noise in the high-frequency domain for practical applications is probably still many years away. The second important conclusion we can draw from Fig. 1 is that there is much to gain in terms of noise reduction by simply cleaning up the small parts in the gear assembly. This may simply involve smoothing out abrupt geometry changes, filling up cutouts and cavities and if possible, grouping and streamlining the small parts. These small modifications do not significantly change the landing gear design, but have the potential to reduce the most offending noise component, namely, the high-frequency noise.

To demonstrate the importance of the high-frequency component, the Boeing 737 landing gear noise data are used to calculate the EPNL. The results are shown in Fig. 2 for the case of flight Mach number of 0.24, which plots the perceived noise levels as a function of the noise emission angle with the total EPNL shown in the box. In this figure, the prediction (circles) is made by using Fink's method [11], which is basically an empirical method derived from small-scale test

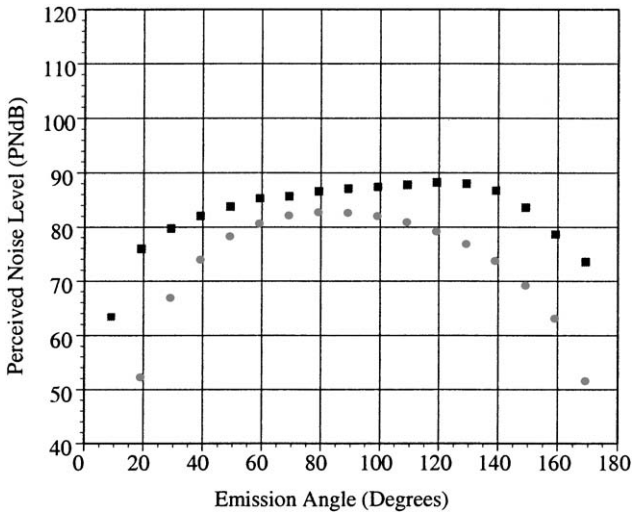

Fig. 2. Comparison of test data with prediction by Fink's empirical model for the Boeing 737 landing gear, showing the underprediction in all directions: ■■■, from test data, and ●●●, from prediction.

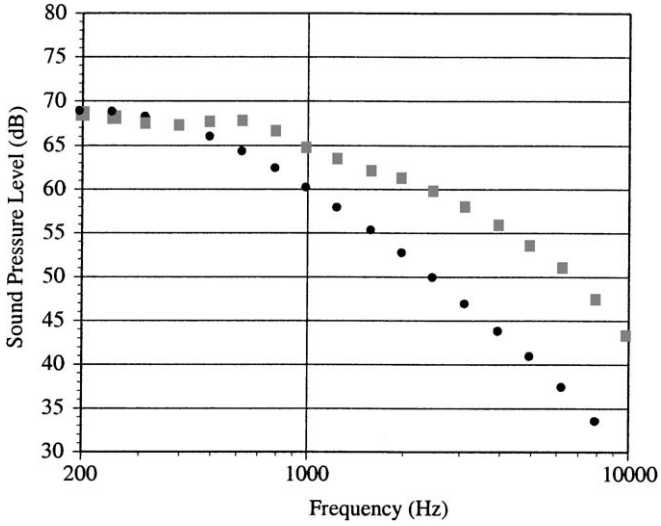

Fig. 3. Comparison of test data with Fink's prediction for Boeing 737 landing gear noise in the overhead direction, showing the large discrepancy between the two at high frequencies: ■■■, from test data, and ●●●, from prediction.

data. It can be seen that the prediction underestimates the noise levels in all directions and the predicted EPNL is 7.8 dB lower than the test data. This huge discrepancy is due to the fact that Fink's prediction only captures the low- and mid-frequency noise. This is further demonstrated in Fig. 3 by the spectral comparison between data and prediction in the overhead location. Clearly,

Fink's prediction agrees well with data at low frequencies but is significantly lower than data at high frequencies.

When the source decomposition illustrated in Fig. 1 is applied to all the test data, the spectral characteristics of the noise in different frequency domains can be clearly revealed. This is shown in Figs. 4–6. In all these figures, the data are plotted in non-dimensional forms with the sound pressure level (SPL) normalized by the overall sound pressure level (OASPL). The normalized

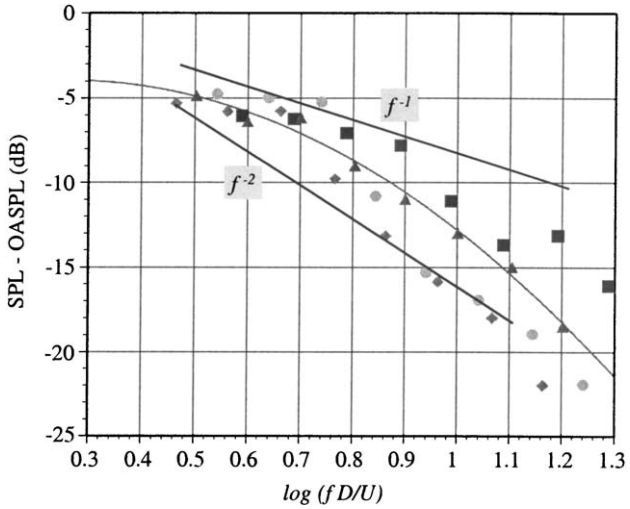

Fig. 4. Normalized noise spectra from landing gear wheels for various flow conditions where the frequency is normalized by the flow velocity U and the wheel diameter D, and the SPL is normalized by the OASPL.

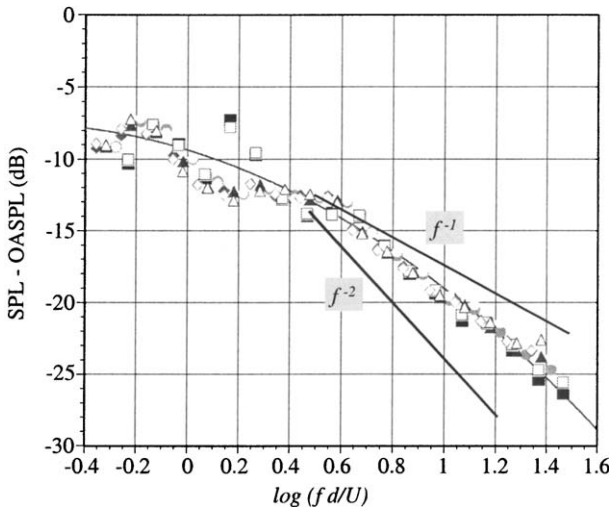

Fig. 5. Normalized noise spectra from landing gear wheels and main struts for various flow conditions where the frequency is normalized by the flow velocity U and the strut diameter d, and the SPL is normalized by the OASPL.

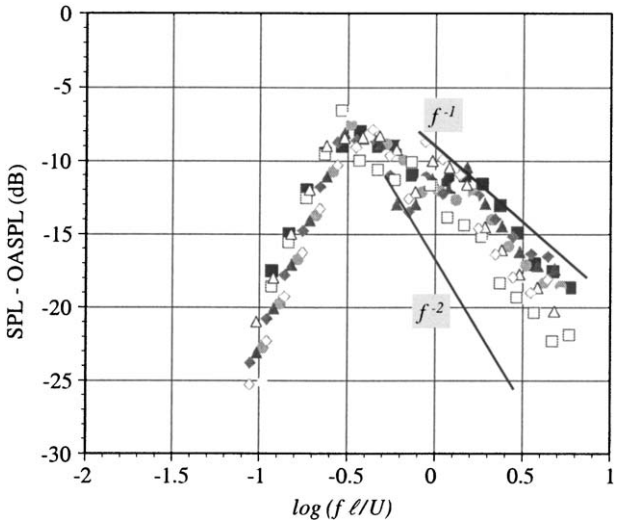

Fig. 6. Normalized noise spectra from small parts of the landing gear assembly for various flow conditions where the frequency is normalized by the flow velocity U and the typical size of the small parts l, and the SPL is normalized by the OASPL.

spectra are plotted as a function of the Strouhal number, defined by the mean flow velocity U for all three cases, but with different length scales; for the very low-frequency noise, the diameter D of the wheels is used as the length scale; the diameter d of the main struts is used for the low-frequency noise; and a typical size l of the small parts in the landing gear assembly is used for the high-frequency component. For the Boeing 737 landing gear, D is approximately 50 inches, d is about 5 inches and l can be taken as 0.5 inch. The flow Mach number in the test ranges from 0.18 to 0.24.

To show the spectral characteristics of the noise, Figs. 4–6 also include the lines indicating the inverse frequency and the inverse squared frequency law. In all the three frequency domains, the data fall in between these two lines. However, the data seem to drift from being close to the inverse square law in the very low-frequency domain, to being in the middle of the two lines in the low-frequency domain, and then to being close to the inverse frequency law in the high-frequency domain. These trends will be used to check the asymptotic results derived in later sections.

3. Farfield sound pressure

We consider the situation where a landing gear assembly moves at constant speed U in the positive x_1 direction, where the coordinate system $\mathbf{x} = \{x_1, x_2, x_3\}$ is fixed in relation to the farfield microphones. The source locations on the landing gear are denoted by $\mathbf{y} = \{y_1, y_2, y_3\}$, which is related to the coordinate system fixed on the landing gear assembly by

$$\mathbf{y} = \boldsymbol{\eta} + \int_0^\tau \mathbf{U}\,\mathrm{d}\tau = \boldsymbol{\eta} + \mathbf{U}\tau, \tag{1}$$

where $\boldsymbol{\eta} = \{\eta_1, \eta_2, \eta_3\}$ is the body-fixed coordinate system, τ is the time measuring the source process and

$$\mathbf{U} = U\hat{x}_1. \tag{2}$$

is the constant velocity in the x_1 direction, the $\hat{}$ on x_1 denoting unit vector.

The farfield sound pressure due to the landing gear assembly can be conveniently expressed by the Ffowcs Williams/Hawking equation [5]. For low Mach number flows, as is the case for landing gear noise applications where the typical flow Mach number is about 0.2, the dominant sound is given by the dipole term due to surface pressure fluctuations. In this case, the sound pressure $p(\mathbf{x}, t)$ can be written as

$$p(\mathbf{x}, t) = \frac{1}{4\pi} \frac{\partial}{\partial x_i} \int_{S(\boldsymbol{\eta})} \frac{n_i p_s(\boldsymbol{\eta}, \tau)}{|(\mathbf{x} - \mathbf{y})(1 - M\hat{x}_1)|} \, \mathrm{d}^2\eta. \tag{3}$$

Here p_s is the surface pressure on the landing gear whose surfaces are collectively denoted by S and we have introduced $M = U/c$ to denote the Mach number with c being the constant sound speed. The unit normal of these surfaces, pointing into the flow, is denoted by n_i, with the repeated indices implying summation. The surface integration is to be carried out in the body-fixed coordinate system η in which the landing gear geometry is time-invariant. The source time τ is now given by the retarded time, defined by the implicit equation

$$\tau = t - |\mathbf{x} - \boldsymbol{\eta} - \mathbf{U}\tau|/c. \tag{4}$$

This equation can be readily solved to find the source time in terms of the coordinate variables and the receiver time

$$\tau = t - \frac{(M^2(x_1 - \eta_1 - Ut)^2 + (1 - M^2)|\mathbf{x} - \boldsymbol{\eta} - \mathbf{U}t|^2)^{1/2} + M(x_1 - \eta_1 - Ut)}{c(1 - M^2)}, \tag{5}$$

which can be used for numerical integration of Eq. (3).

For the purpose of deriving the farfield sound pressure, we assume that the microphones are located far away from the landing gear so that

$$|\mathbf{x}| \gg |\mathbf{y}|. \tag{6}$$

In this case, the implicit equation (4) can be expanded in powers of $1/|\mathbf{x}|$, which leads to

$$\tau \approx t - \frac{|\mathbf{x}|}{c} + \frac{\boldsymbol{\eta} \cdot \mathbf{x}}{c|\mathbf{x}|} + M\hat{x}_1\tau. \tag{7}$$

Thus, the explicit solution for τ becomes

$$\tau \approx \frac{1}{\Delta}\left(t - \frac{|\mathbf{x}|}{c} + \frac{\boldsymbol{\eta} \cdot \mathbf{x}}{c|\mathbf{x}|}\right), \tag{8}$$

where Δ stands for the Doppler factor defined by

$$\Delta = 1 - \frac{\mathbf{U} \cdot \mathbf{x}}{c|\mathbf{x}|} = 1 - M\hat{x}_1. \tag{9}$$

The farfield assumption can be used to simplify the sound pressure given by Eq. (3). Under condition (6), the spatial derivative in Eq. (3) can be replaced with a time derivative

$$\frac{\partial}{\partial x_i} = -\frac{\hat{x}_i}{c}\frac{\partial}{\partial t}, \tag{10}$$

and the spherical spreading of the sound propagation can be approximated as

$$\frac{1}{|\mathbf{x}-\mathbf{y}|} \approx \frac{1}{|\mathbf{x}|}. \tag{11}$$

Thus, the leading order contribution to the farfield sound pressure simplifies to

$$p(\mathbf{x},t) = -\frac{\hat{x}_i}{4\pi c|\mathbf{x}|\Delta}\frac{\partial}{\partial t}\int_{s(\boldsymbol{\eta})} n_i p_s(\boldsymbol{\eta},\tau)\,\mathrm{d}^2\eta. \tag{12}$$

This result can now be converted to the frequency domain by taking Fourier transform on both sides according to the definition

$$\tilde{p}(\mathbf{x},\omega) = \int_t p(\mathbf{x},t)\mathrm{e}^{\mathrm{i}\omega t}\,\mathrm{d}t \quad \text{and} \quad p(\mathbf{x},t) = \frac{1}{2\pi}\int_\omega \tilde{p}(\mathbf{x},\omega)\mathrm{e}^{-\mathrm{i}\omega t}\,\mathrm{d}\omega. \tag{13}$$

where ω is the angular frequency and the $\tilde{}$ denotes quantities in the Fourier transform domain. When Eq. (13) is applied to Eq. (12), the left-hand side gives the Fourier transform of the farfield sound pressure. The transform of the surface pressures at the source time τ can be facilitated by making use of result (8) for the retarded time and

$$\begin{aligned}\int_t p_s(\boldsymbol{\eta},\tau)\mathrm{e}^{\mathrm{i}\omega t}\mathrm{d}t &= \Delta\mathrm{e}^{-\mathrm{i}k|\mathbf{x}|}\mathrm{e}^{-\mathrm{i}k\boldsymbol{\eta}-\hat{\mathbf{x}}}\int_\tau p_s(\boldsymbol{\eta},\tau)\mathrm{e}^{\mathrm{i}\omega_d\tau}\mathrm{d}\tau \\ &= \Delta\mathrm{e}^{-\mathrm{i}k|\mathbf{x}|}\mathrm{e}^{-\mathrm{i}k\boldsymbol{\eta}-\hat{\mathbf{x}}}\tilde{p}_s(\eta,\omega_d).\end{aligned} \tag{14}$$

Here, we have introduced the acoustic wavenumber k to save writing, which is defined by

$$k = \omega/c. \tag{15}$$

In Eq. (14), ω_d is the Doppler-shifted frequency, which is related to ω by

$$\omega_d = \omega\Delta. \tag{16}$$

With this, the farfield pressure (12) becomes

$$\tilde{p}(\mathbf{x},\omega) = \frac{\mathrm{i}k\mathbf{x}_i}{4\pi|\mathbf{x}|}\mathrm{e}^{-\mathrm{i}k|\mathbf{x}|}\int_{S(\boldsymbol{\eta})} n_i\tilde{p}_s(\boldsymbol{\eta},\omega_d)\mathrm{e}^{-\mathrm{i}k_i\boldsymbol{\eta}\cdot\hat{\mathbf{x}}}\,\mathrm{d}^2\eta. \tag{17}$$

Thus, the farfield sound pressure at frequency ω is related to the surface pressures at the Doppler-shifted frequency ω_d. This shift in frequency between the surface pressures and the farfield sound pressure is due to the effects of the motion (with velocity $\mathbf{U}$) of the landing gear assembly. It can be seen from Eq. (17) that the farfield sound and the surface pressures are related not only through the frequency shift associated with the Doppler effect, but also through a phase weighting, characterized by the exponential factor under the integration. Clearly, this phase factor is determined jointly by the frequency parameter k, the landing gear geometry η and the farfield microphone location. The behavior of this phase weighting is very important in the derivation of the asymptotic results in different frequency domains, because it dictates how the

surface pressure integration can be simplified. This will be discussed in detail in the following sections.

4. Low-frequency noise

By low-frequency noise, we mean sound waves whose wavelengths are much longer than any dimension of the landing gear assembly. Because of this, the variations of the surface pressures along the surfaces of the landing gear components are small. For the farfield microphones, small variations in surface pressures can be neglected and the farfield sees the surface pressures as approximately in phase at all surface points. Thus, the noise is generated in this case by the total forces on the landing gear assembly. This is readily understandable from the principles of aerodynamic sound; at low frequencies, the source variations are gradual on the acoustic wavelength scale so that the aggregate effects of the sources are equivalent to simple dipoles whose strengths are furnished by the forces. This is a well-known result that can be derived from the Curie extension [1] of the Lighthill theory [14].

Mathematically, a wavelength much longer than any dimension of the gear means

$$k\boldsymbol{\eta}\cdot\hat{\mathbf{x}} \ll 1 \tag{18}$$

so that the exponential under the integration in Eq. (17) is approximately unity, namely,

$$\mathrm{e}^{-\mathrm{i}k\boldsymbol{\eta}\cdot\hat{\mathbf{x}}} \approx 1, \tag{19}$$

and the surface pressure integration simply becomes

$$\int_{s(\boldsymbol{\eta})} n_i \tilde{p}_s(\boldsymbol{\eta},\omega_d)\,\mathrm{d}^2\eta = F_i(\omega_d), \tag{20}$$

where F_i is the Fourier transform of the total force on the landing gear in the ith direction. On substituting this into Eq. (17), the farfield sound pressure becomes

$$\tilde{p}(\mathbf{x},\omega) = \frac{\mathrm{i}k\hat{x}_i}{4\pi|\mathbf{x}|}\mathrm{e}^{-\mathrm{i}k|\mathbf{x}|}F_i(\omega_d). \tag{21}$$

This result can be used to predict the low-frequency noise if the total forces on the landing gear can be obtained either by experiments or by numerical computation. Because of the low frequencies, the noise is mostly associated with relatively large parts of the landing gear, such as the wheels and the main struts. This makes it feasible for numerical simulation. The simulation can be done by using simplified geometry, which cannot represent the complete flow field of realistic landing gears, but should give reasonably accurate results for the low-frequency noise. Such an attempt has been made recently by Hedges [15], who uses both the unsteady Reynolds-Averaged Navier–Stokes method (URANS) and the Detached Eddy Simulation (DES) [16] to solve the flow field of a simple landing gear and has derived the total forces.

The noise spectrum can be derived from the farfield pressure by multiplying it by its complex conjugate and taking the ensemble average of the result. By denoting the noise spectrum by Π, we then have the definition

$$\Pi(\mathbf{x},\omega) = \left\langle \tilde{p}(\mathbf{x},\omega)\tilde{p}^*(\mathbf{x},\omega)\right\rangle, \tag{22}$$

where the asteroid denotes complex conjugate and the $\langle\rangle$ bracket implies ensemble average. By substituting sound pressure (21) into this, we find that

$$\Pi(\mathbf{x},\omega)=\frac{k^2}{(4\pi|\mathbf{x}|)^2}\left\langle|\hat{x}_i F_i(\omega_d)^2|\right\rangle. \tag{23}$$

This can be further recast into a form that can be conveniently used in cases where the total forces are derived from numerical simulations. In term's of the sound pressure level (SPL), we can define

$$\mathrm{SPL}=10\log\frac{(4\pi|\mathbf{x}|)^2\Pi}{M^2D^2q^2(D/U)^2}=20\log\left\{St_d\frac{|\hat{x}_i F_i(St_d)|}{D^3q/U}\right\}. \tag{24}$$

Here the result is normalized such that the farfield noise is calculated by the Doppler-shifted Strouhal number, defined by

$$St_d=2\pi\omega\Delta D/U, \tag{25}$$

multiplied by the total forces that are themselves normalized by the dynamic head $q=\rho U^2/2$, mean flow velocity U and the wheel diameter D.

To demonstrate the application of this result to predict low-frequency noise from landing gears, we use the results for the total forces computed by solving the flow with numerical simulations for a simple model landing gear [15]. The gear only has the wheels and the main struts. Thus, the flow computed from this model will not be representative of the flow around real landing gears that have a much more complex geometry. However, the small details of the gear mainly contribute to higher-frequency noise. For noise prediction, the simple geometry should be accurate enough for low-frequencies scaling on the wheel diameters. Fig. 7 shows the computed sound pressure levels accoording to Eq. (24) at four different angles, namely, the upstream direction, above the gear, the downstream direction and below the gear (the overhead direction). The Strouhal number in this figure is based on the wheel diameter D and mean flow velocity U. The mean flow has a Mach number of 0.2. For comparison, results from both DES and URANS are shown. For all the cases, the spectra peak around unity Strouhal number. The comparison between the two numerical methods show that URANS predicts a strong tone while DES gives more broadband results. Also, the spectral rolloff above unity Strouhal number is much more gradual for DES than URANS. By comparing these with the experimental data shown in Fig. 4, it seems that the DES-based prediction captures the basic features in the noise spectrum. To see the amplitude prediction, we integrate the spectra to derive the OASPL, which is plotted in Fig. 8 as a function of the directivity angle, measuring from the upstream direction. This figure shows that the predictions from the two flow solvers (DES and URAND) give comparable results in the flight direction, both upstream and down stream. However, the URANS-based method underpredicts the DES-based method by about 5 dB in the overhead direction. We have not been able to pinpoint the source of these discrepancies and further studies are apparently needed.

5. Mid-frequency noise

Except for the low frequencies discussed in the previous section, most other noise components cannot be treated as being generated by the total forces on the landing gear. Instead, they are

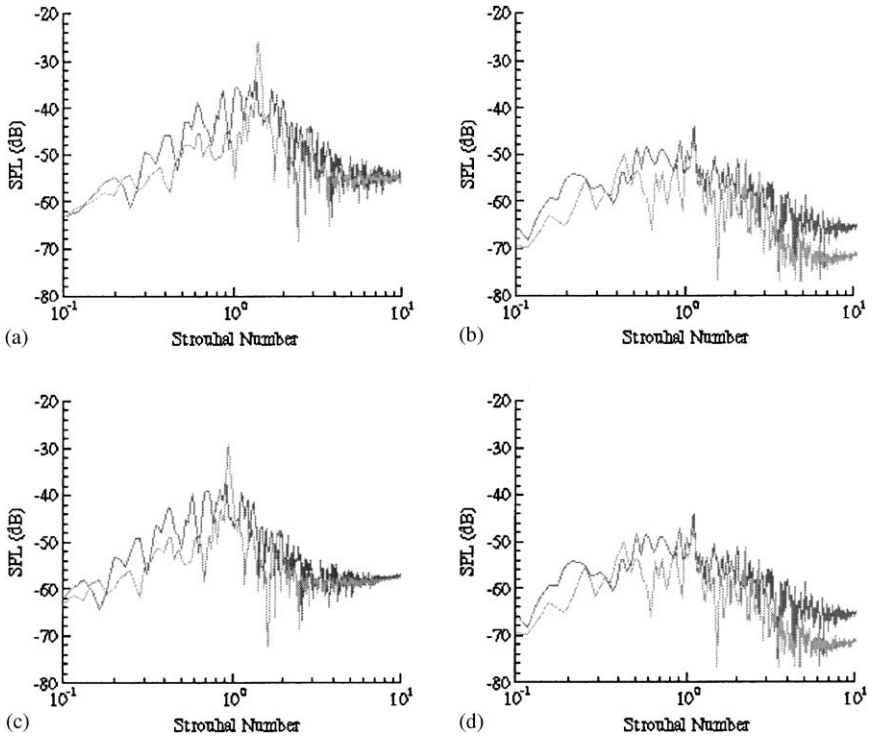

Fig. 7. Low-frequency noise prediction for a simple landing gear consisting of only the wheels and the main struts. The nearfield flow is computed by DES (upper curve) and URANS (lower curve). The Strouhal number is based on the wheel diameter and mean flow velocity. The mean flow Mach number is 0.2. (a) upstream direction, (b) above gear, (c) downstream direction, (d) below gear.

generated by distributed sources. Thus, to calculate the farfield sound pressure, as formulated by, Eq. (17), it is necessary to integrate the pressures on the surfaces of the landing gear assembly. To this end, we assume that the landing gear assembly consists of N components and the surfaces of the components are denoted by S_j ($j = 1, 2, 3, \ldots, N$). Thus, the integral in Eq. (17) over the symbolic surface S, which collectively denotes the surfaces of all the components in the landing gear assembly, can be replaced by a summation of surface integrals over all the components. Result (7) then becomes

$$\tilde{p}(\mathbf{x},\omega) = \frac{\mathrm{i}k\hat{x}_i}{4\pi|\mathbf{x}|}\mathrm{e}^{-\mathrm{i}k|\mathbf{x}|}\sum_{j=1}^{N}\int_{S_j} n_i\tilde{p}_s(\boldsymbol{\eta},\omega_d)\mathrm{e}^{-\mathrm{i}k\boldsymbol{\eta}-\hat{\mathbf{x}}}\,\mathrm{d}^2\eta. \tag{26}$$

To proceed, it is convenient to make a change of variables from the coordinate system η, which moves with the airplane at speed U and globally measures the landing gear assembly, to local coordinates fixed on each of the components. This change of coordinates is illustrated in Fig. 9.

A local coordinate system can facilitate the calculations because landing gear components such as struts usually have long axial dimensions and small cross-sections. A local coordinate system

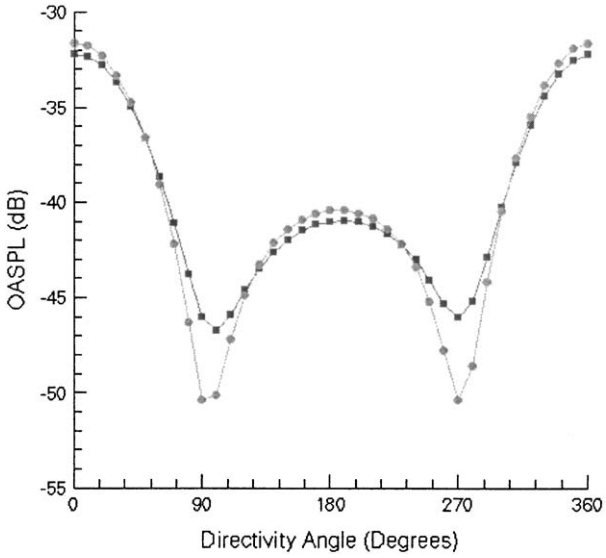

Fig. 8. Farfield directivity of low-frequency noise from wheels and main struts in a landing gear at a mean flow Mach number of 0.2, with unsteady flow calculated by numerical simulation: ■■■, from DES and ●●●, from URANS. The upstream direction is zero degree and the overhead location is at 90°.

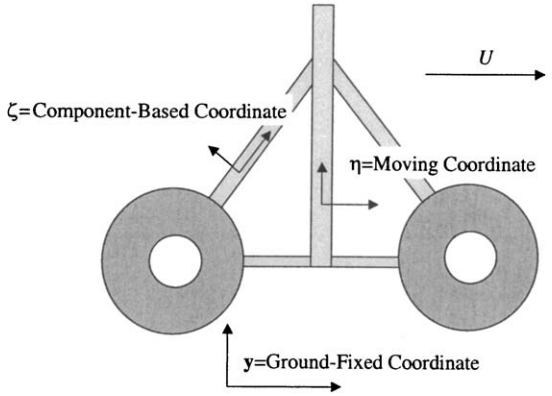

Fig. 9. Illustration of the three different coordinate systems.

enables the surface integral to be carried out separately in the longitudinal and cross-sectional dimension, each of which may allow for different approximations because of their respective length scales. The change of variables can be done in a straightforward way, involving a translation of the origin of the coordinate system onto the jth component and a rotation to align one of the coordinate axes with the longitudinal axis of the component. We choose to denote the middle point of the component by θ_j and specify its longitudinal axis by the polar angle θ_j and azithumal angle ϕ_j. Further, by using $\boldsymbol{\zeta} = \{\zeta_1, \zeta_2, \zeta_3\}$ for the local coordinates, the change of

variables can then be expressed as

$$\boldsymbol{\zeta} = \mathbf{A} \cdot (\boldsymbol{\eta} - \boldsymbol{\eta}_j), \tag{27}$$

where $\mathbf{A}$ is an orthogonal transformation matrix, resulting from the rotation of the coordinate system. The elements of the transformation matrix are given by the inclination angles of the jth component, namely, θ_j and ϕ_j in the form of

$$\mathbf{A} = \begin{pmatrix} \cos\theta_j & \sin\theta_j & 0 \\ -\sin\phi_j \cos\theta_j & \cos\phi_j \cos\theta_j & -\sin\theta_j \\ -\sin\phi_j \sin\theta_j & \cos\phi_j \sin\theta_j & \cos\theta_j \end{pmatrix}. \tag{28}$$

Transformation (27) changes the coordinate system from η to ζ. The latter has its origin located at the middle point η_j and its ζ_3-axis coincides with the longitudinal axis of the jth component. By applying this change of variable to Eq. (26), we have

$$\boldsymbol{\eta} \cdot \hat{\mathbf{x}} = (\boldsymbol{\eta}_j + \mathbf{A}^{-1} \cdot \boldsymbol{\zeta}) \cdot \hat{\mathbf{x}} = \boldsymbol{\eta}_j \cdot \hat{\mathbf{x}} + \boldsymbol{\zeta} \cdot (\mathbf{A} \cdot \hat{\mathbf{x}}), \tag{29}$$

where the power index -1 on $\mathbf{A}$ indicates its inversion and the last step follows from making use of the fact that the transpose of an orthogonal matrix is equal to its inversion. Thus, the surface integral over S_j in Eq. (26) can be rewritten as

$$\mathrm{e}^{-\mathrm{i}k\boldsymbol{\eta}_j \cdot \hat{\mathbf{x}}} \int_{S_j} n_i \tilde{p}_s(\zeta, \omega_d) \mathrm{e}^{-\mathrm{i}k\boldsymbol{\zeta} \cdot \hat{\mathbf{Z}}} \, \mathrm{d}^2\zeta. \tag{30}$$

Here, we have introduced

$$\hat{\mathbf{z}} = \{\hat{z}_1, \hat{z}_2, \hat{z}_3\} = \mathbf{A} \cdot \hat{\mathbf{x}} \tag{31}$$

to denote the unit vector of the radiation direction viewed in the local coordinate system ζ Since the transformation matrix $\mathbf{A}$ is given by the orientation angles of the jth component, namely, θ_j and ϕ_j, as defined in Eq. (28), the unit direction vector (31) is also a function of these orientation angles.

The surface integral over S_j can now be conveniently divided into two line integrals, one along the longitudinal direction and one along the contour of the cross-section of the component. This is illustrated in Fig. 10. Thus, Eq. (30) becomes

$$\mathrm{e}^{-\mathrm{i}k\boldsymbol{\eta}_j \cdot \hat{\mathbf{x}}} \int_{L_j} \int_{C_j} n_i \tilde{p}_s(s, \zeta_3, \omega_d) \mathrm{e}^{-\mathrm{i}k\psi(s)} \, \mathrm{d}s \times \mathrm{e}^{-\mathrm{i}k\zeta_3 \hat{z}_3} \, \mathrm{d}\zeta_3, \tag{32}$$

where L_j and C_j are respectively the length and the cross-section perimeter of the jth component, s is the arc length coordinate of the cross-section contour and we have used ψ save writing. It is defined by

$$\psi(s) = \zeta_1(s)\hat{z}_1 + \zeta_2(s)\hat{z}_2, \tag{33}$$

where $\zeta_1(s)$ and $\zeta_1(s)$ are the coordinates of the cross-section contour as functions of the arc length s.

In the mid-frequency domain, the sound wavelength is much longer than the cross-section dimension, of the landing gear parts, but is short compared with their longitudinal dimension. Take a strut of circular cross-section for example. This means the acoustic wavelength is much

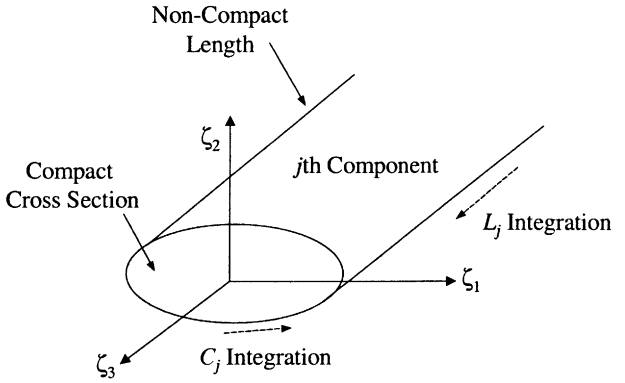

Fig. 10. Illustration of dividing the S_j integration into two line integrals.

larger than the radius of the cross-section but smaller than the length of the strut. In this case, the farfield sound does not see significant variations in surface pressures along the cross-section contour. Thus, for a fixed longitudinal location, the surface pressures along the cross-section contour are approximately in phase and the sound sources are furnished by concentrated forces at this location. In the longitudinal direction, surface pressure variations are significant, because of the much longer length compared with the wavelength, so that the noise sources are distributed along this direction and are described by the statistical properties of the surface pressures.

The above physical descriptions for the mid-frequency noise sources can be expressed in mathematics by the limiting case

$$ka \ll 1, \tag{34}$$

where k is the acoustic wavenumber defined in Eq. (15) and a represents the typical length scale of the cross-section of a component in the landing gear assembly. For a circular cross-section, for example, a can be taken as the radius of the cross-section area. The choice of a and the local coordinate system ζ, then ensures that

$$\zeta_1(s)/a = O(1) \text{ and } \zeta_2(s)/a = O(1), \tag{35}$$

where the symbol $O(\cdot)$ means "of the same order as". Because of this, we have

$$k\psi(s) \ll 1, \tag{36}$$

and the exponential factor in Eq. (32) inside the s-integral can be expanded in the form of

$$\mathrm{e}^{-\mathrm{i}k\psi(s)} = 1 - \mathrm{i}k\psi(s) + o(ka), \tag{37}$$

where we have used the symbol $o(\cdot)$ to mean "of higher order than". From this, the integration over C_j in Eq. (32) is reduced to

$$\int_{C_j} n_i \tilde{p}_s(s, \zeta_3, \omega_d)\{1 - \mathrm{i}k\psi(s) + o(ka)\}\,\mathrm{d}s = F_i^{(j)}(\zeta_3, \omega_d) + \text{higher order terms}. \tag{38}$$

The leading order term on the right-hand side represents the sectional forces (in the frequency domain), indicated by the superscript (j), which also indicates the jth component in the gear

assembly, and defined by the integration of the surface pressures along the cross-section contour. Note that the subscript i is used here to denote the force in the ith direction.

On substituting Eq. (38) into Eq. (32), the leading order contribution to the farfield sound pressure becomes

$$\tilde{p}(\mathbf{x},\omega)=\frac{\mathrm{i}k\hat{\mathbf{x}}}{4\pi|\mathbf{x}|}\mathrm{e}^{-\mathrm{i}k|\mathbf{x}|}\sum_{j=1}^{N}\mathrm{e}^{-\mathrm{i}k\boldsymbol{\eta}_j\cdot\hat{\mathbf{x}}}\int_{L_j}F_i^{(j)}(\zeta_3,\omega_d)\mathrm{e}^{-\mathrm{i}k\zeta_3\hat{z}_3}\,\mathrm{d}\zeta_3. \tag{39}$$

It is clear from this result that the noise sources are distributed along the longitudinal dimension of the landing gear parts with strengths furnished by the sectional forces. The total noise of a landing gear assembly is of course the summation of a collection of dipole distributions with different strengths, locations and orientations, all being determined by the design of the landing gear assembly.

To proceed further, statistical properties of the surface pressures along the length of the gear parts can be utilized to simplify the remaining integral in Eq. (39). This can be done by substituting Eq. (39) into the definition (22) for the sound spectrum, which leads to

$$\begin{aligned}\Pi(\mathbf{x},\omega)=&\frac{k^2}{(4\pi|\mathbf{x}|)^2}\sum_{j=1}^{N}\sum_{n=1}^{N}\mathrm{e}^{-\mathrm{i}k(\boldsymbol{\eta}_j-\boldsymbol{\eta}_n)\cdot\hat{\mathbf{x}}}\\&\times\int_{L_j}\int_{L_n}\left\langle\hat{x}_iF_i^{(j)}(\zeta_3,\omega_d)\hat{x}_mF_m^{(n)*}(\zeta'_3,\omega_d)\right\rangle\mathrm{e}^{-\mathrm{i}k(\zeta_3\hat{z}_3-\zeta'_3\hat{z}'_3)}\,\mathrm{d}\zeta_3\,\mathrm{d}\zeta'_3,\end{aligned} \tag{40}$$

where the ensemble average is taken on the sectional forces because other quantities in the result are all deterministic. Clearly, this ensemble-averaged quantity is the cross-coherence function of the sectional forces, in the longitudinal directions of the components. This result thus essentially states that the noise spectrum is given by the longitudinal cross coherence of the sectional forces, integrated over all the components of the landing gear assembly. The integration can be simplified by noting that the cross coherence is significant only when both ζ_3 and ζ'_3 are on the same component. Mathematically, this means that the summations in Eq. (40) can be set to zero unless $j=n$, in which case, we also have

$$\boldsymbol{\eta}_j=\boldsymbol{\eta}_n\quad\text{and}\quad\hat{z}_3=\hat{z}'_3 \tag{41}$$

By making use of this (40) can be reduced to

$$\Pi(\mathbf{x},\omega)=\frac{k^2}{(4\pi|\mathbf{x}|)^2}\sum_{j=1}^{N}\int_{L_j}\int_{L_j}\left\langle\hat{x}_iF_i^{(j)}(\zeta_3,\omega_d)\hat{x}_mF_m^{(j)*}(\zeta'_3,\omega_d)\right\rangle\mathrm{e}^{-\mathrm{i}k(\zeta_3-\zeta'_3)\hat{z}_3}\,\mathrm{d}\zeta_3\,\mathrm{d}\zeta'_3. \tag{42}$$

The double integral in this result can be further simplified by the fact that there is usually little curvature variation along the longitudinal axis of a typical landing gear component such as a strut. Also, such a typical component usually has a much larger longitudinal dimension than its cross-section dimension, which makes it reasonable to assume spatial homogeneity in the longitudinal direction. For real landing gears, the structure usually has abrupt geometry features such as a step in a long strut that abruptly changes the diameter of the strut. If such a strut is regarded as a single component, the abrupt step will inevitably cause non-homogeneity in the flow characteristics along the length of the strut. However, the strut can also be considered as two

components with different diameters, each having an invariant cross-section along its length. Thus, the surface integration in the formation derived here does not require the surfaces to be smooth. The abrupt geometry features will of course affect the flow and this effect is included in the surface pressures, as input here for noise prediction, and hence, also included in the noise prediction.

If we further regard the flow as statistically stationary, as is usually the case for high Reynolds number (and hence, fully developed turbulent) flows, the longitudinal cross-coherence function can be written in a separable form. By following the arguments of dimensional analysis given by Ffowcs Williams [17], we can assume a form similar to the Corcos model [18,19],

$$\left\langle \hat{x}_i F_i^{(j)}(\zeta_3, \omega_d) \hat{x}_m F_m^{(j)*}(\zeta'_3, \omega_d) \right\rangle = \phi^{(j)}(\omega_d) B(l). \tag{43}$$

Here, $\Phi^{(j)}$ is the auto coherence (e.g., point spectrum) of the sectional forces of the jth component, defined by

$$\Phi^{(j)}(\omega_d) = \left\langle |\hat{x}_i F_i^{(j)}(\zeta_3, \omega_d)|^2 \right\rangle. \tag{44}$$

which usually has a ζ_3-dependence because the landing gear components have finite lengths. This finite length effect, however, can be expected to be small except in regions close to the ends of the components. In most of the surface areas away from the ends, the flow may not differ significantly from one axial location to another so that $\Phi^{(j)}$ can be approximated as invariant in the longitudinal direction. In the cases where the end effects should be included, $\Phi^{(j)}$ can be regarded as the average value along the length of a component. The correlation of the sectional forces in the longitudinal direction is represented by the non-dimensional function B, as a function of the separation distance $l = \zeta_3 - \zeta'_3$ The spatial homogeneity of the flow renders the correlation a function of the separation distance alone.

With Eq. (43) substituted into Eq. (42), the result can be calculated be noting that the correlation function B only depends on the separation distance l. Thus, one of the two ζ_3-integrals can be changed to one over l and the double integral is then trivially reduced to

$$L_j \Phi^{(j)}(\omega_d) \int_0^{L_j} B(l) \mathrm{e}^{-\mathrm{i}kl\hat{z}_3} \mathrm{d}l. \tag{45}$$

By comparing the l-integral in this with the definitions of the Fourier transform in Eq. (13), it is clear that for an infinitely long component, the l-integral would be the wavenumber spectrum of B at the acoustic wavenumber modified by the convection effects. This implies that it is the sonic component in the wavenumber spectrum of the sectional force correlation that is responsible for the farfield radiation. For finite length L_j, the l-integration is over a finite length so that some other wavenumbers are also scattered into sound by the end effects.

By collecting all above the results, the farfield noise spectrum (40) is now reduced to

$$\Pi(\mathbf{x}, \omega) = \frac{k^2}{(4\pi|\mathbf{x}|)^2} \sum_{j=1}^{N} L_j \Phi^{(j)}(\omega_d) \int_0^{L_j} B(l) \, \mathrm{e}^{-\mathrm{i}kl\hat{z}_3} \, \mathrm{d}l. \tag{46}$$

This relates the farfield noise to the auto-spectra of the sectional forces on the components of the landing gear assembly. The summation over the N components indicates that the noise from the

individual component is statistically added (energy addition). The addition is, however, weighted by the lengths of the individual components and the longitudinal correlation of the sectional forces. It is also clear from Eq. (46) that the relation between farfield sound and the forces is frequency shifted, due to the Doppler effect.

In result (46), the effects of flow correlation in the longitudinal direction are accounted for by the quantity $B(l)$. There have been extensive studies in the past concerning the correlation function for flows over surfaces with no curvature variations and many analytical forms have been proposed to model such a correlation. For example, an exponential expression can be proposed following Ffowcs Williams [17], in the form of the Corcos model [18,19],

$$B(l) = \mathrm{e}^{-l/l_0 + \mathrm{i}l\omega_d/V_c}. \tag{47}$$

Here, the correlation falls off exponentially with the separation distance l and is characterized by the correlation length scale l_0, which is a function of frequency (approximately inversely proportional to frequency). The imaginary part of the exponent is introduced to account for the effects of flow convection along the longitudinal direction, with the convection velocity denoted by V_c. This convection occurs because the longitudinal axes of the components are not always perpendicular to the flow direction. Thus, the mean flow convects in both the longitudinal and the circumferencial direction, the velocity in the latter direction being denoted by U_c.

With Eq. (47) assumed for the correlation function, the l-integration in Eq. (46) can be carried out explicitly with the result

$$\int_0^{L_j} B(l)\,\mathrm{e}^{-\mathrm{i}kl\hat{z}_3}\mathrm{d}l = (l_0/\mu)\left(\mathrm{e}^{\mu L_j/l_0} - 1\right), \tag{48}$$

where we have introduced μ to save writing, which is defined by

$$\mu = \mathrm{i}(\omega_d l_0/V_c)(1 - \hat{z}_3 V_c/c) - 1, \tag{49}$$

which is a weak function of frequency, where c is the constant sound speed.

With the above results, the only remaining quantity that is needed for the noise prediction is the auto-spectrum of the sectional forces. For arbitrary landing gear components, this quantity has not been systematically studied and future work is apparently needed. Experimental measurements are clearly feasible (by using Kulites on the surfaces, for example) and are crucial in developing empirical models. Numerical simulations are also feasible. In this approach, the gear components can be divided into a few groups (say, circular struts, rectangular beams, etc.), each of which contains components of similar shapes but differing sizes. By computing the surface pressures of these individual components within fully turbulent flows, the auto-spectra of the sectional forces can be derived, as functions of other parameters in the problem. The numerically generated data can then be analyzed to derive semi-empirical formulas. Before it is feasible to simulate landing gear flows for practical applications, the component-based approach seems to be the one that makes best use of numerical simulations and leads to tools that can be used for engineering applications.

Once the auto-spectra of the sectional forces are derived, either numerically or empirically, landing gear noise prediction can be done easily by Eq. (46). As a demonstration, we use some empirical results from published literature for the quantity $\Phi^{(j)}$. To this end, we note that the sectional force can be written as the circumferentially averaged forces per unit length multiplied

by the length of the cross-section perimeter, namely,

$$\hat{x}_i F_i^{(j)}(\zeta_3, \omega_d) = \int_{C_j} \hat{x}_i n_i \tilde{p}_s(s, \zeta_3, \omega_d)\, \mathrm{d}s = \hat{\mathbf{x}} \cdot \mathbf{n}_f C_j p_c(\omega_d), \tag{50}$$

where C_j is used to denote the length of the perimeter of the cross-section, $\mathbf{n}_f$ denotes the unit vector of the sectional forces and p_c is the circumferentially averaged surface pressure. From this, Eq. (44) becomes

$$\Phi^{(j)}(\omega_d) = (\hat{\mathbf{x}} \cdot \mathbf{n}_f)^2 C_j^2 \langle |p_c(\omega_d)|^2 \rangle. \tag{51}$$

Here, we have introduced the circumferentially averaged surface pressure because the auto-spectra of this quantity have been studied in the past for circular cross-sections, which is applicable here to circular section struts. For example, Willmarth and Yang [20] measured this auto-spectra and showed that

$$\langle |p_c(\omega_d)|^2 \rangle = 6\pi \times 10^{-6} \frac{1}{\omega a / U_c} \frac{0.12 \rho^2 U_c^3 a}{1 + (0.6 \omega a / U_c)^2}, \tag{52}$$

where a is the radius of the cross-section and U_c is the flow convection velocity in the direction normal to the axis of the struts. With this substituted into Eq. (51) and the result in turn substituted into Eq. (46), the noise due to the circular struts in the low-frequency domain can be found provided the dimensions and orientations of the struts are given. To demonstrate the frequency features, Fig. 11 plots the spectrum from one individual strut. The spectrum is broadband in nature with a maximum at a Strouhal number of about 0.2, the Strouhal number being based on the radius a and the flow convection velocity U_c. For a group of struts with differing radii, the spectrum would be flatter, showing more broadband features, because the

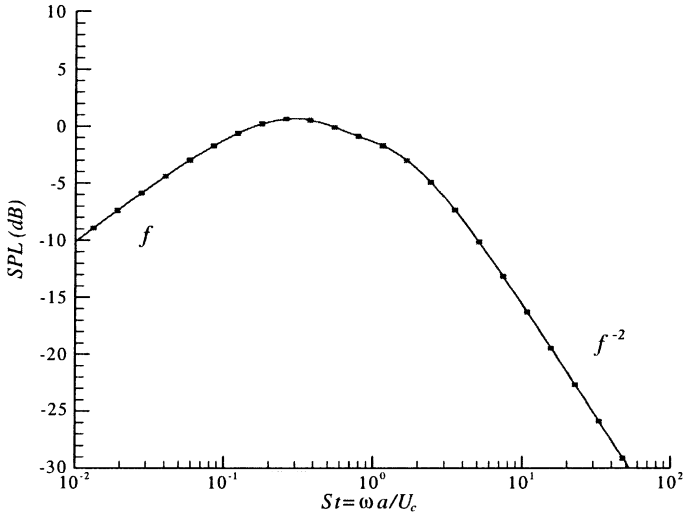

Fig. 11. Spectral characteristics of low-frequency noise form an individual circular strut. The Strouhal number is based on the radius of the circular cross-section and the streamwise convection velocity U_c.

maximum for each individual strut would appear at different frequencies. Fig. 11 also shows that the spectrum is proportional to frequency well below the maximum hump and inversely proportional to the square of frequency well above the peak frequency. The latter seems to be quite consistent with the data shown in Fig. 5, where measurements are shown to collapse very well onto a trend line between the inverse frequency and the inverse frequency squared. Note that the data in Fig. 5 are shown in one-third-octave band spectra, which explains why the prediction in Fig. 11 falls off more rapidly.

6. High-frequency noise

As shown in Section 2, high-frequency noise is a significant contributor to landing gear noise. This component of landing gear noise is generated by sources with characteristic length scales comparable or smaller than the physical dimensions of the gear parts. In terms of the source distributions furnished by the surface pressures, as formulated by Eq. (17), the farfield sees significant phase variations in the source distributions in all directions. Thus, no part of the sources can be treated as concentrated dipoles. This corresponds to the limiting case

$$ka \gg 1 \tag{53}$$

when k is large. Since the cross-section coordinates are of the same order as a, as indicated by Eq. (35), we have in the high-frequency domain

$$k\psi(s) \gg 1, \tag{54}$$

where $\psi(s)$ is defined by Eq. (33). Under this condition, it is clear that the integrand of the C_j-integral in Eq. (32) is highly oscillatory, because of the exponential factor. This naturally calls for the application of the method of stationary phase, which is a standard technique in asymptotic analysis for dealing with integrals with a highly oscillatory integrand [21]. The method leads to a result expressed in terms of values of the integrand at the stationary points. Without repeating the details of the derivation, which can be found in standard textbooks, we reduce the C_j-integral in Eq. (32) to

$$\int_{C_j} n_i \tilde{p}_s(s, \zeta_3, \omega_d)\, \mathrm{e}^{-\mathrm{i}k\psi(s)}\, \mathrm{d}s = n_i(s_0)\tilde{p}_s(s_0, \zeta_3, \omega_d)\left\{\frac{2\pi}{k|\psi''(s_0)|}\right\}^{1/2} \mathrm{e}^{-\mathrm{i}k\psi(s_0)\pm\mathrm{i}\pi/4}, \tag{55}$$

where s_0 is the arc coordinate at the stationary point and the double prime on $\psi(s)$ indicates the second order derivative with respect to s. If there is more than one stationary point, the result is understood to be a sum over all the stationary points. The definition of the stationary point is

$$\psi'(s_0) = 0, \tag{56}$$

where the prime means differentiation with respect to argument. Clearly, a stationary point has a vanishing gradient of the phase function.

The meaning of this method now becomes clear. Since the integrand on the left-hand side of Eq. (55) is highly oscillatory, the contributions to the integration from all the elements essentially cancel each other, except at the stationary point where the gradient of the phase function vanishes

so that the mutual cancellation between the elements is not complete. The residue of this incomplete cancellation is the result on the right-hand side of Eq. (55). This also precisely reflects the physics of high-frequency, distributed noise sources. The source distributions have rapid phase variations so that their contributions to the farfield noise largely cancel each other. The radiation is then only from the sources whose phase variation is zero. These surviving sources are located at exactly the stationary points defined by Eq. (56). It is also of interest to note that this source cancellation effect degrades the order of the sources from dipoles to quadrupoles. This, however, does not necessarily imply less efficient radiation, in terms of Mach number dependence, for example, because the sources are of high frequencies and are mostly non-compact. It is known that non-compact sources follow a Mach number scaling that is quite different from that for compact sources and almost invariant with flow Mach number [3,8].

Result (55) can now be substituted into Eq. (32), which in turn can be substituted into Eq. (26), leading to the high-frequency sound in the form of

$$\tilde{p}(\mathbf{x},\omega)=\frac{\hat{x}_i}{|\mathbf{x}|}\left\{\frac{k}{8\pi \mathrm{i}}\right\}^{1/2}\mathrm{e}^{-\mathrm{i}k|\mathbf{x}|}\sum_{j=1}^{N}\mathrm{e}^{-\mathrm{i}k\boldsymbol{\eta}_j\hat{\mathbf{x}}}\int_{L_j}n_i(s_0)\frac{\tilde{p}_s(s_0,\zeta_3,\omega_d)}{|\psi''(s_0)|^{1/2}}\mathrm{e}^{-\mathrm{i}k\{\psi(s_0)+\zeta_3\hat{z}_3\}}\,\mathrm{d}\zeta_3. \tag{57}$$

This result relates the farfield noise to the surface pressures at the stationary points on the landing gear surface. The physical meaning of the stationary points can be found from their definition (56) with $\psi(s)$ given by Eq. (33). These two lead to

$$\psi'(s_0)=\zeta'_1(s_0)\hat{z}_1+\zeta'_2(s_0)\hat{z}_2=0, \tag{58}$$

where again the prime means first order derivative with respect to the indicated argument. The meaning of this becomes clear once it is recognized that $\boldsymbol{\zeta}=\{\zeta_1,\zeta_2,\zeta_3\}$ are the local coordinates fixed on the jth component of the gear assembly with the ζ_3-axis coinciding with the longitudinal axis of this component (see Figs. 9 and 10). Thus, ζ_1 and ζ_2, as a function of the arc length coordinate s, are the coordinates of the cross-section perimeter in parametric form. The first order derivatives of the two are related to the unit tangent vector of the perimeter by the definition

$$\mathbf{t}(\mathrm{s}_0)=\left\{\zeta'_1(s_0),\zeta'_2(s_0)\right\}/\left[(\zeta'_1)^2+(\zeta'_2)^2\right]^{1/2}. \tag{59}$$

From this, the condition (58) can be re-written as

$$\mathbf{t}(s_0)\cdot\hat{\mathbf{z}}=0, \tag{60}$$

where $\hat{\mathbf{z}}$ is the unit vector of the farfield microphone location in the component-based coordinate system, namely,

$$\hat{\mathbf{z}}=\{\hat{z}_1,\hat{z}_2\}. \tag{61}$$

It is now clear that a stationary point is a location on the landing gear surface where the surface tangent is normal to the direction from this location to the farfield microphone. This is illustrated in Fig. 12. According to the definitions of surface curvature, it is known that the quantity $\psi''(s_0)$ is related to the curvature at the stationary point.

Since the meaning of the stationary points is clear now, the result for the farfield sound given by Eq. (57) can be further simplified. Because the cross-section is usually invariant in the longitudinal direction for most landing gear parts, the quantities involving s_0 in the integrand of the ζ_3-integral

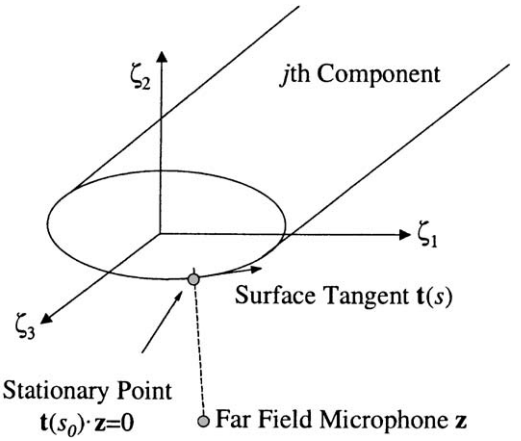

Fig. 12. Illustration of the component-based coordinate system and the physical meaning of the stationary points on the component surface.

in Eq. (57) can be regarded as independent of ζ_3, and hence be moved outside of the integration. The remaining calculation can proceed in a manner similar to the derivations in the previous section. This involves the substitution of the farfield pressure (57) into definition (22) for the noise spectrum. By making use of the ensemble average and by assuming that surface pressures are not correlated for different landing gear components, we find that

$$\Pi(\mathbf{x},\omega)=\frac{k}{8\pi|\mathbf{x}|^2}\sum_{j=1}^{N}\frac{(\hat{x}_i n_i(s_0))^2}{|\psi''(s_0)|}\int_{L_i}\int_{L_j}\left\langle\tilde{p}_s(s_0,\zeta_3,\omega_d)\tilde{p}_s^*(s_0,\zeta'_3,\omega_d)\right\rangle \mathrm{e}^{-\mathrm{i}k(\zeta_3-\zeta'_3)\hat{z}_3}\,\mathrm{d}\zeta_3\,\mathrm{d}\zeta'_3. \tag{62}$$

Now, to further evaluate the integral involving the two-point correlation of the surface pressures, the same statistical arguments as those in the previous section apply, which lead to

$$\left\langle\tilde{p}_s(s_0,\zeta_3,\omega_d)\tilde{p}_s^*(s_0,\zeta'_3,\omega_d)\right\rangle=\Phi_p^{(j)}(\omega_d)B(l) \tag{63}$$

where $\Phi_p^{(j)}(\omega_d)$ is the auto-spectrum of the surface pressures at the stationary point and B is the correlation function in the longitudinal direction, which we assume to have the same form as that used in the previous section. With this, the noise spectrum (62) becomes

$$\Pi(\mathbf{x},\omega)=\frac{k}{8\pi|\mathbf{x}|^2}\sum_{j=1}^{N}\frac{(\hat{x}_i n_i(s_0))^2}{|\psi''(s_0)|}L_j\Phi_p^{(j)}(\omega_d)\int_0^{L_i}B(l)\mathrm{e}^{-\mathrm{i}kl\hat{\mathbf{z}}_3}\,\mathrm{d}l. \tag{64}$$

This result predicts the farfield noise in the high-frequency domain, requiring as input the surface pressure spectrum at the stationary point and the longitudinal correlation of the surface pressures.

The surface pressure spectra need to be derived either by empirical method or numerical simulations. The most easily and most widely studied surface pressure spectrum is that on a rigid cylinder. The best data on this seem to be that due to Markowitz [22], who finds the empirical formula

$$\Phi_p^{(j)}(\omega)=6\pi\times10^{-6}\rho^2U_c^3a\left[1+(0.6\omega a/U_c)^2\right]^{-1}, \tag{65}$$

where again a is the radius of the cylinder cross-section and U_c is the local flow convection velocity in the direction normal to the cylinder axis. With results like this and by using Eq. (48) for the longitudinal correlation, the farfield noise can be easily predicted. For a single strut with circular cross-section, the spectrum behaves similarly to that shown in Fig. 11, namely, broadband in nature with a maximum hump at about the Strouhal number of 0.2. The spectrum is also proportional to frequency well below the maximum hump and falls off inversely with frequency squared well above the maximum frequency. These similar features for the two frequency components are consistent with the data shown in Figs. 5 and 6, which only show slightly different trends. These slight differences in spectral trends are very likely to show up from the summation in results (46) and (64). This is because in a landing gear assembly, the number of main struts is certainly different from the number of small parts and the size distributions of these two groups of components are also different. The spectral shape of the noise components will also de determined by the correlation functions. The two particular forms given here are used as examples of how the noise prediction can be done once this information is available. More elaborate models may probably need to be developed for practical implementation of the prediction methodology.

7. Conclusions

In this paper, we have developed a statistical model for landing gear noise prediction. The model decomposes the farfield noise into three different frequency domains and derives asymptotic results for each frequency domain by making use of the phase behavior of the sources, which is controlled mostly by the ratio of the wavelength to the typical dimension of the landing gear components. In each frequency domain, this ratio is used to simplify the phase function of the sources, which, together with some statistical descriptions of the surface pressures on the landing gear, has enabled us to derive analytical solutions for the farfield sound pressure. We have also shown, by analyzing the experimental data from a full-scale B737 landing gear test, that the noise contributions in these three different frequency domains are dominantly from three respective groups of landing gear components, namely, the wheels, the main struts and the small details. Because of this, we believe that the asymptotic results derived in this report capture the main features of landing gear noise, both in spectral characteristics and in noise levels. The limited validation by and comparison with data seem to confirm this.

There are many attractive features in the analytical results derived in this paper. Simplicity is definitely one of them. This is most attractive for engineering applications where quick turn-around time is required. Obviously, the computational requirements for the noise calculations, once the statistical properties of the surface pressures are known, are trivial since the results are all explicit analytical expressions. The requirements for the surface pressure information are also small; none of the three frequency domain predictions requires complete descriptions of the surface pressures. For very low and low frequencies, only the total forces and the sectional forces are needed, while for high frequencies, surface pressures are needed only at a few locations on the gear. For numerical simulations, this will definitely lessen the burden of data storage. For physical experiments, it can quite significantly cut the cost of mapping the surface pressures, especially for wind tunnel tests where the relative positions of the farfield microphones and the landing gear are fixed. For flight test where the landing gear moves in relation to the ground microphones, a series

of surface positions may have to be monitored. Even in these cases, significant cost saving can be achieved by avoiding extensive surface pressure measurements.

The frequency domain decomposition also points to simple ways to derive the surface pressures. Take numerical simulations for example. Instead of attempting full-blown computations for realistic landing gears, which will probably remain an extremely difficult, if not impossible, task for the foreseeable future, we can make use of the fact that different groups of landing gear parts generate noise in different frequency domains. For low and mid frequencies, the radiation from the wheels and the main struts dominates so that the nearfield flow simulation can afford to ignore the small details on the gear. Such a simplified landing gear simulation has become quite feasible in recent years. For high frequencies, the small details of the gear assembly are important for noise generation, but it seems to be reasonable to assume that there is little correlation between the small parts for high frequencies. It can be further assumed that the turbulent mean flow around the gear assembly is dominantly determined by the large components. Thus, the nearfield simulation for high frequencies can be done for individual components. In this case, the gear parts can be catalogued into groups of similar shapes, such as circular struts and rectangular beams. The surface pressure properties on these individual parts (in the high-frequency domain) can be obtained by computing the results with the parts placed in a turbulent flow, which can be the mean flow from the low-frequency, simple gear simulation. Simulations with an isolated strut or beam should be quite possible with currently available computing capability and the results of such simulations can be parameterized to derive the surface pressure properties as a function of component shape, size, orientation and flow conditions. This is in fact a part of the future work that needs to be done in order to bring the results of this paper into practical applications.

Acknowledgements

The work reported here was conducted under NASA Contract NAS1-97040, under Task 2 of the Advanced Subsonic Technology (AST) program. The task was managed by the Fluid Mechanics and Acoustics Division of NASA Langley Research Center. Dr. C.L. Streett was the technical monitor. The author would like to thank Dr. Streett for his support.

The author would also like to thank R. Stoker, P.R. Spalart and L. Hedges of the Boeing Company for freely sharing their test data and CFD results with the author and for many productive discussions on landing gear noise.

References

[1] N. Curie, The influence of solid boundaries upon aerodynamic sound, *Proceedings of the Royal Society (London) A* 231 (1955) 505–514.

[2] J.E. Ffowcs Williams, Hydrodynamic noise, *Annual Review of Fluid Mechanics* 1 (1969) 197–222.

[3] D.G. Crighton, Basic principles of aerodynamic noise generation, *Progress in Aerospace Sciences* 16 (1) (1975) 31–96.

[4] D.G. Crighton, Airframe noise, in: *Aeroacoustics of Flight Vehicles: Theory and Practice*, NASA RP-1258, Vol. 1, 1991, pp. 391–447.

[5] J.E. Ffowcs Williams, D.L. Hawkings, Sound generation by turbulence and surfaces in arbitrary motion, *Philosophical Transactions of Royal Society (London) A* 264 (1969) 321.
[6] Y.P. Guo, A model for slat noise generation, AIAA Paper 97-1647, 1978.
[7] Y.P. Guo, Application of Ffowcs Williams/Hawkings equation to two dimensional problems, *Journal of Fluid Mechanics* 403 (2000) 201–221.
[8] Y.P. Guo, A discrete vortex model for slat noise prediction, AIAA Paper 2001-2157, 2000.
[9] R.W. Stoker, Landing gear noise test report. NASA Contract NAS1-97040, 1997.
[10] H. Heller, W. Dobrzynski, Sound radiation from aircraft wheel-well/landing-gear configuration, *Journal of Aircraft* 14 (8) (1977) 768–774.
[11] M.R. Fink, Noise component method for airframe noise, *Journal of Aircraft* 17 (2) (1980) 99–105.
[12] W. Dobrzynski, H. Buchholz, Full-scale noise testing on Airbus landing gears in the German dutch wind tunnel, AIAA Paper 97-1597 1997.
[13] R. Sen, R.W. Stoker, Airframe Noise Test of a 0.063-scale 777 Model: Test Report, NASA Contract NAS1-97040, 1999.
[14] M.J. Lighthill, On sound generated aerodynamically I. General theory, *Proceedings of the Royal Society (London) A* 211 (1952) 564–587.
[15] L.S. Hedges, A. Travin, P.R. Spalart, Detached-eddy simulations over a simplified landing gear, *Journal of Fluids Engineering* 124 (2) (2002) 413–423.
[16] P.R. Spalart, W-H Jou, M. Strelets, S.R. Allmaras, Comments on the feasibility of LES for wings, and on a hybrid RANS/LES approach, *First AFOSR International Conference on DNS/LES*, 1997.
[17] J.E. Ffowcs Williams, Boundary-layer pressures and the Corcos model: a development to incorporate low-wavenumber constraints, *Journal of Fluid Mechanics* 125 (1982) 9–25.
[18] G.M. Corcos, Resolution of pressure in turbulence, *Journal of the Acoustical Society of America* 35 (1963) 192–199.
[19] G.M. Corcos, The resolution of turbulent pressures at the wall of a boundary layer, *Journal of Sound and Vibration* 6 (1967) 59–70.
[20] W.W. Willmarth, C. Yang, Wall pressure fluctuations beneath an axially symmetric turbulent boundary layer on a cylinder, ONA Project 02149, University of Michigan, 1969.
[21] D.G. Crighton, A.P. Dowling, J.E. Ffowcs Williams, M. Hekle, F.G. Leppington, *Modern Methods in Analytical Acoustics*, Springer, Berlin, 1992.
[22] A.E. Markowitz, Turbulent boundary layer wall pressure fluctuations and wall acceleration measurements on a long flexible wall cylinder towed at sea, NUSC TR5305, New London, 1976.